Lorentz force electrical impedance tomography using pulse compression technique*

Zhi-shen Sun(孙直申)[1,2,3], Guo-qiang Liu(刘国强)[1,2,†], and Hui Xia(夏慧)[1]

[1] *Institute of Electrical Engineering, Chinese Academy of Sciences, Beijing* 100190, *China*
[2] *University of Chinese Academy of Sciences, Beijing* 100049, *China*
[3] *Université Lyon, Université Claude Bernard Lyon* 1, *Centre Léon Bérard, Inserm, LabTAU UMR*1032, *F*-69003, *Lyon, France*

(Received 17 July 2017; revised manuscript received 24 August 2017; published online 20 October 2017)

Lorentz force electrical impedance tomography (LFEIT) combines ultrasound stimulation and electromagnetic field detection with the goal of creating a high contrast and high resolution hybrid imaging modality. In this study, pulse compression working together with a linearly frequency modulated ultrasound pulse was investigated in LFEIT. Experiments were done on agar phantoms having the same level of electrical conductivity as soft biological tissues. The results showed that: (i) LFEIT using pulse compression could detect the location of the electrical conductivity variations precisely; (ii) LFEIT using pulse compression could get the same performance of detecting electrical conductivity variations as the traditional LFEIT using high voltage narrow pulse but reduce the peak stimulating power to the transducer by 25.5 dB; (iii) axial resolution of 1 mm could be obtained using modulation frequency bandwidth 2 MHz.

Keywords: Lorentz force electrical impedance tomography, Hall effect imaging, magneto-acousto-electrical tomography, linear frequency-modulation, pulse compression

PACS: 43.80.+p, 72.55.+s, 73.50.Rb **DOI:** 10.1088/1674-1056/26/12/124302

1. Introduction

The electrical conductivity of biological tissue produces a relatively good contrast among different biological tissues in the human body. For instance, the muscle tissue is almost ten times as conductive as the liver tissue.[1] For the tissue in different pathological stages, for example, the normal and tumor liver tissue, its electrical conductivity changes by more than 50 percent.[2] This characteristic has aroused interests of many researchers. One of the methods thus developed is electrical impedance tomography (EIT),[3] in which the electrical current is injected into the subject through each of one set of electrodes and the generated electrical current density distribution is detected using the remaining electrodes. But this method suffers from low spatial resolution because of the ill-posed problem in the inverse problem.[4] Sonography, another well developed medical imaging technique, can focus the ultrasound beam to the focal zone, therefore obtaining high spatial resolution. However, the acoustic impedance varies within a few percent among different biological soft tissues,[5] thus sonography has the disadvantage of low contrast. Lorentz force electrical impedance tomography (LFEIT)[6–9] combines the ultrasound stimulation used in sonography and the electrical field measurement used in EIT by putting the biological tissue in the magnetic field, vibrating the tissue using ultrasound pulses and detecting the electrical signal — induced by Lorentz force — inside the biological tissue. LFEIT can therefore get the high contrast electrical conductivity variation distribution with the same spatial resolution as that of sonography.

In LFEIT, conventionally, a high-voltage, narrow pulse signal is used to stimulate the transducer to generate the ultrasound pulse. This approach suffers from the problem of imposing high peak instantaneous power on the transducer, which lessens the normal usage lifetime of the transducer. Therefore, demands for reducing the peak stimulating power to the ultrasound transducer while maintaining the differentiating capability of conventional LFEIT are immediately apparent. Recently, we succeeded in imaging the electrical conductivity variation distribution using LFEIT with low instantaneous peak power to the transducer by combining linearly frequency modulated (LFM) ultrasound pulse with coherent frequency demodulation technique.[10]

In this study, we explored the use of pulse compression technique in LFM LFEIT. The pulse compression technique originated in radar signal processing,[11] where it was used to increase the radar detection range while maintaining the peak transmitting power. In recent years, it had been investigated a lot and applied in medical ultrasound[12–15] and ultrasonic non-destructive testing.[16] In this work, first, the theory of application of pulse compression in LFM LFEIT was presented. Then, experiments were done to demonstrate the feasibility and performance of this method.

*Project supported by the National Natural Science Foundation of China (Grant Nos. 51137004 and 61427806), the Scientific Instrument and Equipment Development Project of Chinese Academy of Sciences (Grant No. YZ201507), and the China Scholarship Council (Grant No. 201604910849).

†Corresponding author. E-mail: gqliu@mail.iee.ac.cn

© 2017 Chinese Physical Society and IOP Publishing Ltd

2. Theory

2.1. Measured current signal in LFEIT

In LFEIT, as shown in Fig. 1, the collected current signal can be expressed as[6]

$$I_{\mathrm{LF}} = \alpha \iiint_{x_1}^{x_2} \left[\frac{B_y}{\rho(x)} \frac{\partial \sigma(x)}{\partial x} \int_{-\infty}^{t} p(\tau, x)\, \mathrm{d}\tau \right] \mathrm{d}x\mathrm{d}y\mathrm{d}z, \quad (1)$$

where $\sigma(x)$ is the sample's local electrical conductivity, $\rho(x)$ the sample's local density, B_y the magnetic induction density along e_y, and $p(t,x)$ the ultrasound pressure field.

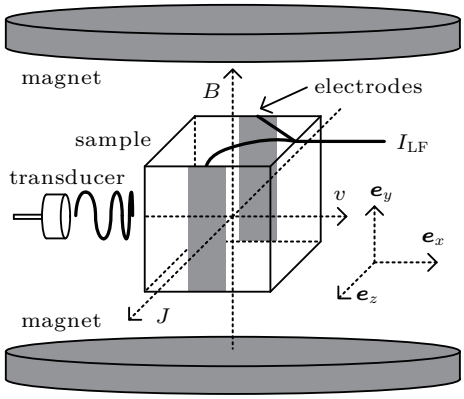


Fig. 1. The positive and negative ions in the conductive medium deviate in opposite directions as they move back and forth due to the ultrasound stimulation, which ultimately generates electrical current density in the conductive medium. One part of the induced current is collected by the electrodes (I_{LF}) while the remaining stays within the sample.

The integrand in Eq. (1) is zero at places where the gradients of $\sigma(x)$ along e_x are zero, and the integration over these places does not contribute to the integral. Only integration over the variations of $\sigma(x)$ in the ultrasound propagation path contributes to the integral and is reflected in the detected current signal. Therefore, inversely, the detected LFEIT current signal could be used to reconstruct the range information of the electrical conductivity variations. By keeping the transducer transmitting ultrasounds along e_x, moving the transducer in equal steps along e_z, collecting the LFEIT signals at each spot and joining together all the LFEIT signals, a B-scan image which represents the electrical conductivity variation distribution is produced.

2.2. LFEIT with LFM ultrasound wave and pulse compression

The implementation of pulse compression in LFEIT is shown in Fig. 2. The stimulating signal to the ultrasound transducer is of the form as Eq. (2), with the frequency sweeping linearly from f_0 to $f_0 + \Delta f$.

$$T_x = A_0 \cos\left\{ 2\pi \left[f_0 + \frac{\Delta f}{2T}(t - kT_m) \right] (t - kT_m) + \phi_0 \right\}, \quad kT_m \ll t < kT_m + T, \quad (2)$$

where A_0 is the amplitude of the transmitted signal, f_0 the initial frequency, T the frequency modulation period, Δf the modulation bandwidth, T_m the LFM pulse repeat period, and ϕ_0 the initial phase.

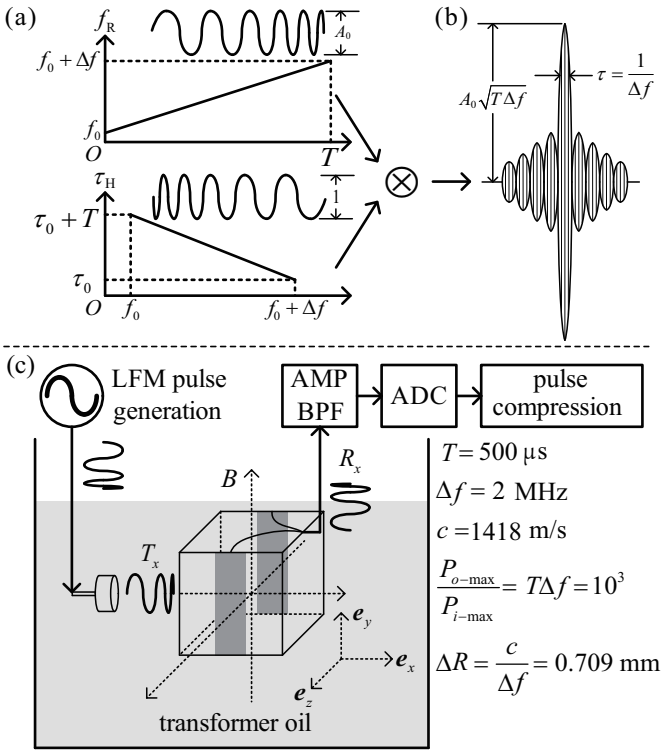


Fig. 2. LFEIT using pulse compression technique. (a) Frequency characteristics of the R_x and the group delay (τ_{H}) of the pulse compression filter function H. (b) The output signal of the pulse compression filter. (c) Schematic diagram of LFM LFEIT system using pulse compression.

Although the stimulating signal to the ultrasound transducer has flat amplitude, the transmitted ultrasound pulses from the transducer do not have flat amplitude because the amplitude-frequency response of the ultrasound transducer is not flat within the modulation frequency band f_0 to $f_0 + \Delta f$. But the frequency of the transmitted ultrasound pulse signal still has the characteristics of linearly increasing with respect to time because the group delay of the ultrasound transducer is constant in the frequency band f_0 to $f_0 + \Delta f$. The induced current signal, as shown in Eq. (1), is the time-domain integral of the ultrasonic pressure signal. Because the time-domain integral of one sinusoid results in a sinusoid of the same frequency, the resulting current signal has the same instantaneous frequency as the ultrasound pressure signal. Also, because T_x's frequency increases with time, the integral of ultrasound pressure also introduces amplitude variation into R_x's amplitude. Nevertheless R_x's instantaneous frequency (Fig. (2a)) increases linearly with the same frequency modulation rate as the stimulating signal. To sum up, we obtain R_x as Eq. (3)

$$R_x = A(t) \cos\left\{ 2\pi \left[f_0 + \frac{\Delta f}{2T}\left(t - kT_m - \frac{R}{c} \right) \right] \times \left(t - kT_m - \frac{R}{c} \right) + \phi_0 \right\}, \quad kT_m + \frac{R}{c} \ll t < kT_m + \frac{R}{c} + T, \quad (3)$$

where $A(t)$ accounts for the overall amplitude-frequency response of the transducer, the ultrasound propagating medium and the acousto-electrical transforming system, R is the range of the electrical conductivity variation and c the ultrasound propagation speed.

The selected matched pulse compression filter has the impulse response of the form:

$$h(t) = A_0 \cos\left\{2\pi\left[f_0 + \Delta f - \frac{\Delta f}{2T}(t - kT_m)\right] \times (t - kT_m) + \phi_0\right\}, \quad kT_m \ll t < kT_m + T. \tag{4}$$

The $h(t)$'s instantaneous frequency decreases linearly at the same absolute rate as R_x, and the group delay (τ_H) of the transfer function ($H(f)$) of the pulse compression filter decreases linearly at the rate of $T/\Delta f$ (Fig. 2(a)). The group delay characteristics of the compression filter enables it to compress R_x into a narrow pulse with high effective peak power (Fig. 2(b)). The temporal width (measured at appropriate point) of the compressed pulse equals $1/\Delta f$. The peak instantaneous power of the pulse increases by a ratio of $T\Delta f$. Instead of deriving the analytical solution of the compressed pulse, numerical simulation is done to get a view of the compressed signal as shown in Fig. 3. The generation of the LFEIT signal (of duration 500 μs) has taken into consideration the uneven amplitude-frequency response of the transducer and the integral in the acousto-electrical transformation. As shown in Fig. 3, although the compressed pulse's waveform degrades from one sharp peak into two peaks due to R_x's varying amplitude, LFEIT signal's width is compressed a lot and a high axial resolution is achieved.

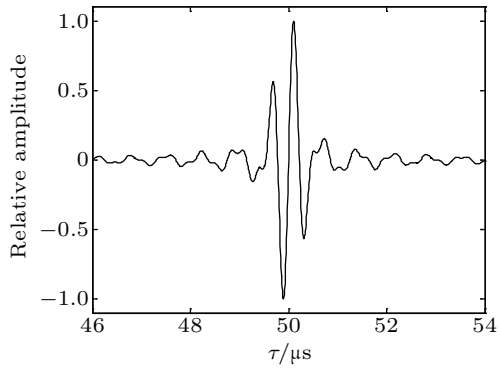


Fig. 3. LFEIT signal-induced by electrical conductivity variation locating at 70.9 mm from the transducer - is compressed. The ultrasound propagation speed of 1418 m/s in the medium is used here.

3. Experimental setup and methods

The schematic diagram of the experimental setup was shown in Fig. 2(c). The LFM pulse was generated using arbitrary waveform generator (Keysight 33600A) with modulation time of 500 μs, sweep frequency ranging from 1.4 MHz to 3.4 MHz (so the axial resolution is about 0.7 mm), pulse repeat frequency (PRF) of 100 Hz, and the LFM signal was amplified by power amplifier (NF HSA4101) to 60Vpp to stimulate the transducer. The transducer used was the Olympus C306, which was a flat transducer with the element size of diameter 1.27 cm and the −6-dB bandwidth between 1.4 MHz and 3.38 MHz.

Two cylindrical permanent magnets made from NdFeB N45 and having size of 15 cm×3 cm (diameter×height) were used to generate the static magnetic field. They were placed coaxially, along the same direction and with a distance of 8.3 cm between each other. Numerical calculation using Maxwell 16.0 showed that the magnetic field within the central cube of 125 cm^3 between the magnets was about 260 mT and the magnetic field homogeneity was greater than 94.5%.

Copper sheets, which were 1 mm thick and had dimensions of 25 mm×50 mm ($X \times Y$), attached closely to the lateral sides of the sample to detect the induced electrical current within the sample (Fig. 2(c)). The detected LFEIT current signal by electrodes was firstly amplified using Olympus PREAMP 5662 by 34 dB, then high-pass and low-pass filtered, and finally fed to oscilloscope (Tektronix DPO2014B) for AD conversion with rate 125MSPS. Coherent averaging by 512 times was adopted before AD conversion. The collected digital LFEIT signal then was transferred to PC for pulse compression using MATLAB.

The samples used in the experiments were agar phantoms made from the mixture of edible salt, agar and water. The quantity ratio between the agar and the water was 1g agar every 100 ml water. The electrical conductivity of the phantom was controlled by changing the salt concentration, for instance, salt concentration of 1.351×10^{-3} g/ml corresponding to electrical conductivity of 0.2 S/m. Before saturation, the electrical conductivity of the phantom changed linearly with the salt concentration. The electrical conductivity of the phantoms used in experiments was in the range of 0.2 S/m–0.4 S/m, which were the typical values of normal biological tissues.

When doing experiments, the transducer and the samples of agar phantom were immersed in the transformer oil in the tank (Fig. 2(c)) so that the ultrasound could propagate into the sample with less attenuation.

4. Results and discussion

4.1. LFEIT signal from a three-layer saline agar phantom

The first experiment was done on the sample of a three-layer agar phantom to verify the feasibility of the method. The three layers were of the same size of 10 mm×50 mm×75 mm ($X \times Y \times Z$). The electrical conductivities of each layer of the agar phantom were 0.2 S/m, 0.2 S/m, and 0.4 S/m respectively. The three layers were placed closely next to each other. Plastic

films (0.015-mm thick) were used to separate neighboring layers so that Na^+ and Cl^- could not move from one layer into another layer (Fig. 4(a)). When doing experiments, the distance between the transducer and the front interface of the agar phantom was 75 mm. Figure 4(b) shows the final compressed pulse signal. Three pulses were induced and corresponded to the 1st, the 3rd, and the 4th interfaces of the phantom respectively, but there was no pulse produced due to the 2nd interface, which demonstrated that the pulses were induced by the electrical variations rather than the acoustic variations.

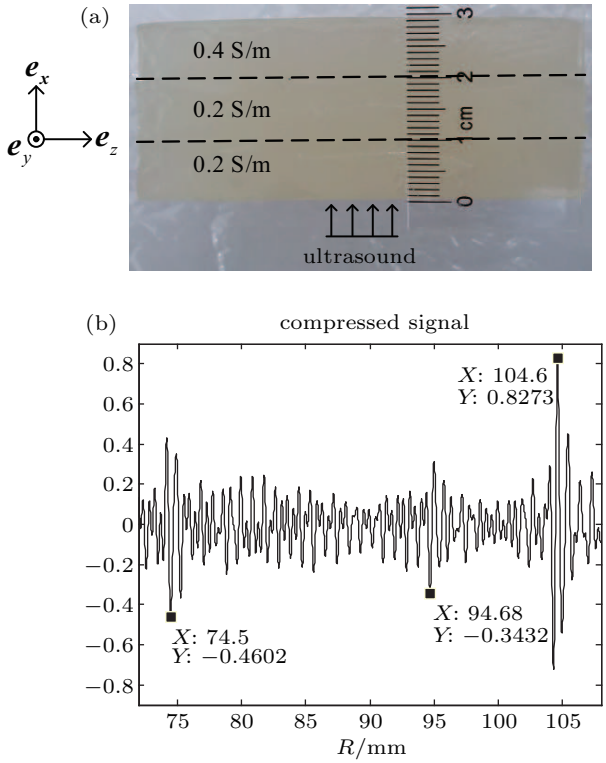


Fig. 4. (color online) (a) Top side view of the 3-layer agar phantom. The electrical conductivities for the three layers were 0.2 S/m, 0.2 S/m, and 0.4 S/m respectively. Each layer was 10 mm in e_x, and the distance from the transducer to the 1st interface of the agar phantom was 75 mm. (b) Compressed LFEIT pulse signals induced by the 1st, the 3rd and the 4th interfaces of the phantom.

4.2. B-scan image of multi-shaped agar phantoms

The second experiment was done with two multi-shaped agar phantoms. The first agar phantom had dimensions of 30 mm×50 mm×75 mm ($X \times Y \times Z$), and it had a rectangular through hole along e_y - of dimensions of 10 mm×50 mm×15 mm ($X \times Y \times Z$) - in the center of the phantom (Fig. 5(a)). The electrical conductivity of the phantom was 0.2 S/m. B-scan image of the phantom was produced by moving the transducer in the e_z direction from −20 mm, in 1 mm step, to 20 mm and putting the compressed pulse signal together, as shown in Fig. 5(b). In Fig. (5(b), evidently, four electrical conductivity variations along e_x can be recognized, which correspond to the four interfaces of the agar phantom. The lateral sizes of the inner recognized interfaces were approximately 15 mm. Two abnormalities occurred due to the velocity difference of ultrasound in the phantom and in the transformer oil: i) the distances between the 1st and the 2nd interfaces and between the 3rd and the 4th interfaces were shorter than the distance between the 2nd and the 3rd interfaces; ii) the reconstructed 4th interface was broken into 3 parts. This was because the ultrasound propagates faster and shorter delay is generated for the same distance in the agar phantom than in the transformer oil, and when the ultrasound velocity in transformer oil was used to reconstruct the propagation delay in the agar phantom, the reconstructed range was shorter than the real range.

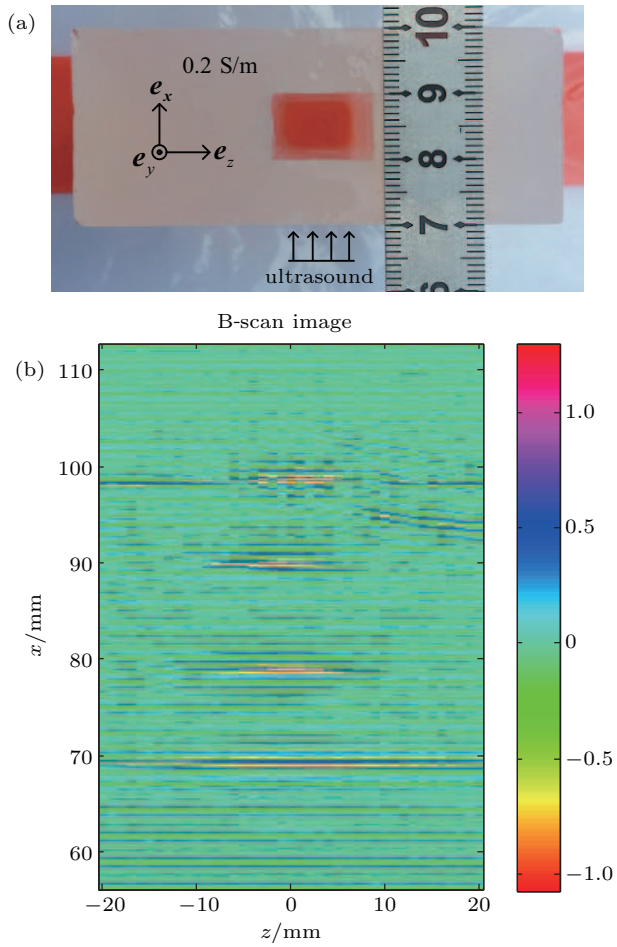


Fig. 5. (color online) B-scan image of the phantom with a rectangular through hole in the center. (a) Top side view and dimensions of the agar phantom. The electrical conductivity of the agar phantom was 0.2 S/m. The middle rectangular hole was of dimensions of 10 mm×50 mm×15 mm ($X \times Y \times Z$). (b) B-scan image of the phantom by LFEIT using pulse compression.

The second multi-shaped agar phantom had dimensions of 30 mm×50 mm×75 mm ($X \times Y \times Z$) and consisted of three layers. In the middle part of the phantom, the 1st and the 3rd layers were sunken while the 2nd layer was protruding along e_x. The dimensions of the protruding area were 15 mm×50 mm×15 mm ($X \times Y \times Z$), as shown in Fig. 6(a). The electrical conductivities of the three layers were respectively 0.2 S/m, 0.4 S/m, and 0.2 S/m. Plastic films (0.015-mm thick) were also placed between adjacent layers to keep the Na^+ and Cl^- concentration in each layer. B-scan image

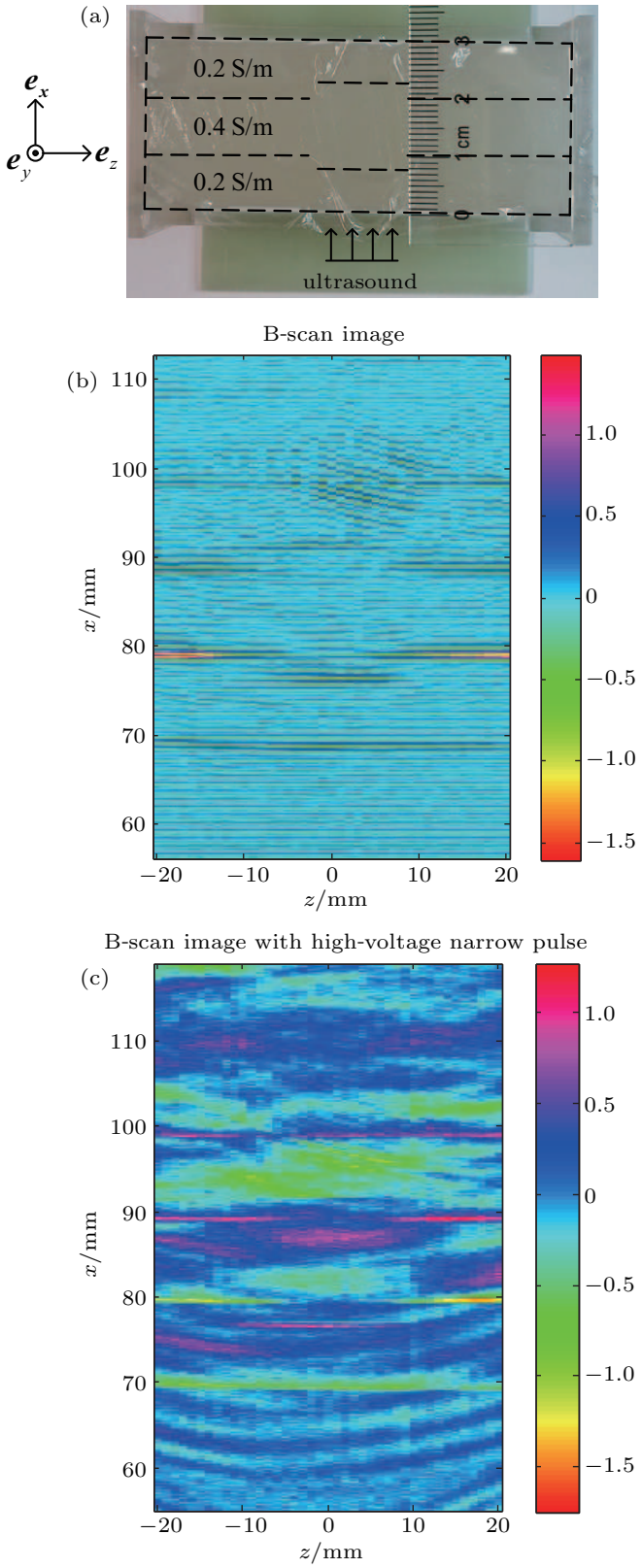


Fig. 6. (color online) The multi-shaped 3-layer agar phantom and its B-scan images. (a) The top-side view and dimensions of the phantom. (b) B-scan image of the agar phantom by LFEIT using pulse compression. (c) B-scan image reconstructed by conventional LFEIT using high-voltage narrow pulse.

of electrical variations of this agar phantom was produced and shown in Fig. 6(b), from which the outline of the interfaces between the three layers of the agar phantom could be recognized clearly. The recognized dimensions of the protruding area of the middle layer in $\boldsymbol{e}_x$ and $\boldsymbol{e}_z$ were approximately 15 mm and 15 mm respectively, which agreed well with the real dimensions. The B-scan image constructed by conventional LFEIT using 400Vpp narrow pulse signal to stimulate the transducer was also presented (Fig. 6(c)). Making a comparison between Fig. 6(b) and 6(c), we can obtain that, even though the peak power of the stimulating signal to the transducer was 25.5 dB lower in LFEIT using pulse compression than in conventional LFEIT using high-voltage narrow pulse, LFEIT using pulse compression was comparable with conventional LFEIT in performance of detection of electrical conductivity variations.

4.3. Verification of axial resolution

The final experiment was done with an agar phantom of dimensions of 30 mm×50 mm×75 mm ($X \times Y \times Z$) and with two slots (Fig. 7(a)). In $\boldsymbol{e}_x$, the first slot had a dimension of 1mm while the second one had a dimension of 2 mm. Both slots had a dimension of 15 mm in $\boldsymbol{e}_z$. The electrical conductivity of the agar phantom was 0.5 S/m. The distance between the transducer and the front interface of the agar phantom was 70 mm. The sample's B-scan image by LFEIT using pulse compression technique was shown in Fig. 7(b). From the B-scan image (Fig. 7(b)), we can recognize the front and back interfaces of each slot clearly. Axial resolution of 1 mm therefore was verified using the experimental setup.

The lateral resolution of the imaging method of LFEIT using pulse compression is determined by the −6-dB beam width of the transducer used. In all the above experiments, Olympus C306, a flat transducer with a large beam width, was adopted. Nevertheless, the lateral dimension of the recognized interfaces inside the phantoms did not widen much. Future experiments with focal transducers Olympus C304 of which the −6-dB beam width can be as small as 2.77 mm are planned.

Different from those in conventional LFEIT using high-voltage narrow pulse or in LFM LFEIT using coherent demodulation, the signal obtained by LFEIT using pulse compression has high sidelobes (Fig. 3), which is caused by the uneven amplitude of the detected LFEIT signal from the same electrical conductivity variation. This problem undermined the axial resolution, and effort towards it through compensated compression filter function is ongoing.

LFM LFEIT using pulse compression samples the detected signal directly and then processes the digital data with the matched pulse compression filter rather than converts the detected LFEIT signal's frequency down to the base-band and then samples the low frequency signal. Therefore, LFM LFEIT using pulse compression requires high sampling rate and high data transmission rate, and its cost of realization is high. But with the popularity of the high-speed ADCs and micro-processors, its cost decreases, which makes this scheme

another choice for LFEIT using LFM ultrasound pulse.

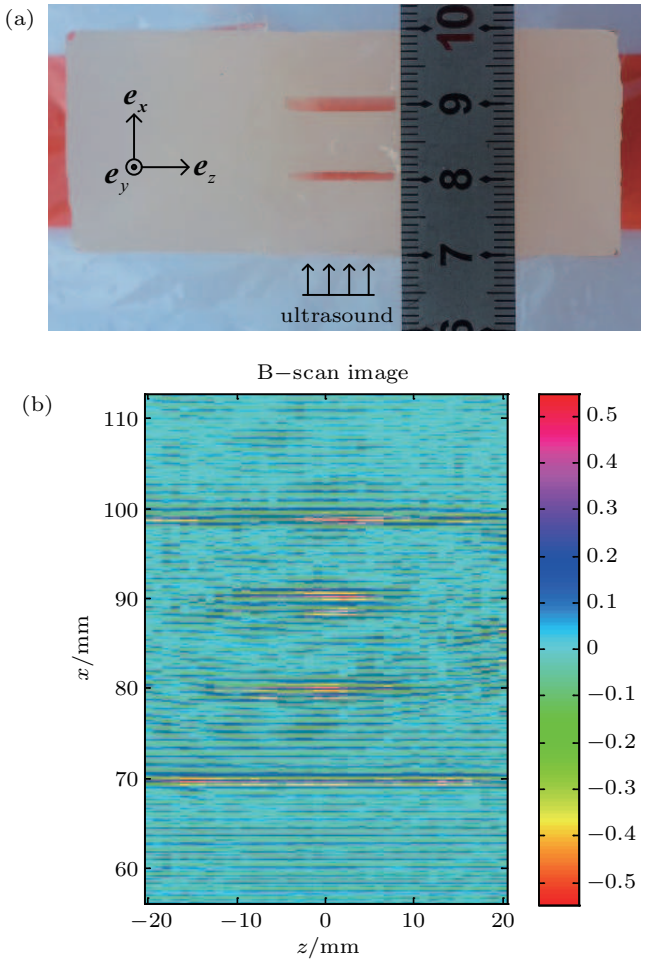


Fig. 7. (color online) B-scan image of the agar phantom with two slots. (a) Top-side view and dimensions of the agar phantom. (b) B-scan image of the agar phantom by LFEIT using pulse compression.

5. Conclusion

We carried out an in-depth study of the application of pulse compression technique in LFM LFEIT. Although, in the frequency range 1.4 MHz–3.4 MHz, the ultrasound transducer's amplitude-frequency response was not flat, and integral of the ultrasound pressure signal also produced variation in the amplitude of the induced LFEIT current signal, the LFEIT signal after pulse compression still exhibited as a narrow pulse. Experiments with agar phantoms of low electrical conductivity demonstrated the feasibility and performance of LFEIT using pulse compression. The 3-layer agar phantom experiment verified the viability of LFEIT using pulse compression to precisely locate the electrical conductivity variations. The multi-shaped agar phantom experiments showed that LFEIT using pulse compression, similar to LFEIT using coherent demodulation method which was another work of the project, could achieve comparable performance with conventional LFEIT using narrow high-voltage pulse, while lowering the peak stimulating power to the ultrasound transducer by 25.5 dB. Finally, the narrow slot phantom experiment demonstrated that, using sweep frequency bandwidth of 2 MHz, LFEIT using pulse compression could differentiate electrical conductivity variations 1 mm axially apart.

References

[1] Gabriel C, Gabriel S and Courhout E 1996 *Phys. Med. Biol.* **41** 2231
[2] Haemmerich D, *et al.* 2003 *Physiol. Meas.* **24** 251
[3] Cheney, Margaret, David Isaacson and Jonathan C Newell 1999 *SIAM Rev.* **41** 85
[4] Ammari H and Kang H 2004 *Reconstruction of Small Inhomogeneities from Boundary Measurements*, Springer Science & Business Media
[5] Goss S A, Johnston R L and Dunn F 1978 *J. Acoust. Soc. Am.* **64** 423
[6] Wen H, Shah Jatin and Balaban R S 1998 *IEEE Trans. Biomed. Eng.* **451** 119
[7] Montalibet A, Jossinet J and Matias A 2001 *Ultrasonic Imaging* **23** 117
[8] Haider S, Hrbek A and Xu Y 2008 *Physiol Meas* **29** S41
[9] Grasland-Mongrain P, *et al.* 2013 *Irbm* **34** 357
[10] Sun Z S, *et al.* "Lorentz Force Electrical Impedance Tomography Using Linearly Frequency-Modulated Ultrasound Pulse", IEEE Trans. Ultrason. Ferroelect. Freq. Control, under Review
[11] Cook C E 1960 *Proceedings of the IRE* **48** 310
[12] Gan T H, et al. 2001 *Ultrasonics* **39** 181
[13] Misaridis T and Jensen J A 2005 *IEEE Trans. Ultrason, Ferroelect, Freq. Control* **52** 177
[14] Misaridis T and Jensen J A 2005 *IEEE Trans. Ultrason, Ferroelect, Freq. Control* **52** 192
[15] Misaridis T and Jensen J A 2005 *IEEE Trans. Ultrason, Ferroelect, Freq. Control* **52** 208
[16] Ricci M, *et al.* 2012 *Insight-Non-Destructive Testing and Condition Monitoring* **54** 91